Advance Sustainable Science, Engineering and Technology (ASSET)
Vol. 8, No.4, October 2026, pp. 02604016-01 ~ 02604016-010
ISSN: 2715-4211 DOI: https://doi.org/10.26877/asset.v8i4.2915

Loading-Dependent Physicochemical Characteristics of $LiMn_2O_4$ Composites with Plasma-Modified and Ammonia-Functionalized Rice Husk Carbon

Harianingsih[1*], Deni Fajar Fitriyana[2], Januar Parlaungan Siregar[3], Agung Budiwirawan[4], Ari Dwi Nur Indriawan[2], Suryo Wiroyudho Wibowo[1], Rizky Ilham Fadzillah[1], Nabila Khoirunisa[1]

[1]Department of Chemical Engineering, Faculty of Engineering, Universitas Negeri Semarang, Kampus Sekaran Gunungpati, Semarang 50229, Central Java, Indonesia

[2]Department of Mechanical Engineering, Faculty of Engineering, Universitas Negeri Semarang, Kampus Sekaran Gunungpati, Semarang 50229, Central Java, Indonesia

[3]Faculty of Mechanical and Automotive Engineering Technology, Universiti Malaysia Pahang Al-Sultan Abdullah, Pekan 26600, Pahang, Malaysia

[4]Department of Civil Engineering, Faculty of Engineering, Universitas Negeri Semarang, Kampus Sekaran Gunungpati, Semarang 50229, Central Java, Indonesia

*harianingsih@mail.unnes.ac.id

Abstract. This study investigates $LiMn_2O_4$ composites incorporated with nitrogen-functionalized rice husk-derived carbon as a sustainable secondary phase for cathode material development. Rice husk carbon was prepared through carbonization, acid-assisted activation, plasma treatment, and ammonia functionalization, then mechanically blended with $LiMn_2O_4$ at 2, 3, and 4 wt.% to obtain LMO-NC2, LMO-NC3, and LMO-NC4, respectively. FTIR analysis showed absorption bands at approximately 3390, 1625, 1400, 1008, 832, 702, and 460 cm^{-1}, corresponding to O–H, C=C, C=N, Si–O, and Mn–O-related vibrations. The minimum transmittance decreased from LMO-NC2 to LMO-NC4, particularly at ~1400 cm^{-1} from 17.13% to 16.01%, indicating stronger carbon/nitrogen-related surface features. SEM revealed layered $LiMn_2O_4$, fine carbon deposits, interparticle voids, and agglomeration. XRD showed characteristic spinel $LiMn_2O_4$ indexed to the (111), (311), (222), (400), (331), (511), and (440) planes. BET adsorption volume increased from 160 cc/g for LMO-NC2 to approximately 169 and 176 cc/g for LMO-NC3 and LMO-NC4 at P/P_0 = 0.31. These findings demonstrate the potential of rice husk-derived carbon for sustainable $LiMn_2O_4$ composite design, supporting responsible consumption and production under SDG 12.

Keywords: composite; $LiMn_2O_4$; plasma modified; rice husk carbon; SDG 12

(Received 2026-10-28, Revised 2026-07-10, Accepted 2026-07-24, Available Online by 2026-08-29)

1. Introduction

Carbonaceous additives are commonly introduced into cathode composites to improve particle contact, electronic pathways, and interfacial stability [1]. Conventional carbon materials such as carbon black, graphite, graphene, and carbon nanotubes have been widely used, but their production may involve high cost, complex processing, or energy-intensive routes. Biomass-derived carbon provides an attractive alternative because it combines functional material development with waste valorization [2]. Rice husk is particularly promising because it is abundant, inexpensive, and contains both carbonaceous and silica-rich components. Through carbonization, activation, and surface modification, rice husk can be converted into porous carbon suitable for composite material applications [3].

The development of biomass- and waste-derived materials is consistent with current directions in sustainable engineering. Anis et al. reported that biomass feedstock granulometry affects the thermophysical and mechanical properties of charcoal briquettes, demonstrating that particle characteristics and processing conditions strongly influence the performance of biomass-based materials [4]. This principle is relevant to rice husk-derived carbon because particle morphology, porosity, and surface condition can affect its interaction with $LiMn_2O_4$ in composite systems. This principle is also relevant for rice husk-derived carbon used in electrode composites, where precursor treatment and particle distribution may influence surface area, porosity, and contact behavior [5]. Similarly, Fitriyana et al. showed that waste-derived materials require controlled processing to achieve useful properties. Surface functionalization is also important for improving biomass-derived carbon [6]. Acid-assisted activation can reduce inorganic impurities and improve surface accessibility, while plasma treatment can generate reactive sites and defects. Subsequent ammonia exposure may introduce nitrogen-containing surface functionalities, which can modify the interaction between carbon and oxide particles [7].

Rice husk-derived materials may also retain silica-related features, which are important in spectroscopic and structural interpretation. Nur Qudus et al. examined KOH-modified rice husk ash and showed that calcination and impregnation conditions affect FTIR, SEM, BET, and XRD characteristics [8]. Despite growing interest in biomass-derived carbon and $LiMn_2O_4$-based composites, limited attention has been given to plasma-assisted nitrogen functionalization of rice husk-derived carbon as an additive for $LiMn_2O_4$ composite cathode materials. Many studies have focused either on $LiMn_2O_4$ modification using conventional carbon sources or on biomass carbon preparation without integration into cathode composites. This creates a research gap at the intersection of sustainable carbon synthesis, plasma surface engineering, and $LiMn_2O_4$ composite design. Therefore, this study aims to prepare and characterize $LiMn_2O_4$ composites containing nitrogen-functionalized rice husk-derived carbon at 2, 3, and 4 wt.% loadings.

2. Methods

2.1. Materials

Rice husk was used as the biomass precursor and obtained from a local rice-milling facility at Wonosalam, Demak, Central Java, Indonesia. Hydrochloric acid Merck 1.00314.2500, was used for acid-assisted purification and activation, while ammonia gas Merck 1054321011, was used as the nitrogen source for post-plasma functionalization. Deionized water, CAPSM 15189, was used throughout washing and neutralization steps. Commercial $LiMn_2O_4$ powder, CAS 1304-85-4, supplied by a Chemical Engineering Laboratory, Universitas Negeri Semarang, was used as the cathode-active material. All chemicals were used as received without further purification.

2.2. Preparation of Rice Husk Charcoal

The raw rice husk was repeatedly washed with deionized water to remove adhering soil, dust, and soluble surface impurities. The cleaned biomass was then oven-dried (Chemical Engineering Laboratory, Universitas Negeri Semarang, Semarang, Indonesia) at 105 °C for 2 h to reduce residual

moisture prior to thermal treatment. Carbonization was carried out in a tubular furnace (Thermo Fisher Scientific, Waltham, MA, USA) at 500 °C for 1 h under an inert atmosphere. After cooling to room temperature under the same atmosphere, the resulting rice husk charcoal was ground using a mortar and sieved (Argoci, Xi'an, China) through a 250 μm mesh to obtain a homogeneous particle size fraction for subsequent activation [9].

2.3. Acid-Assisted Activation of Rice Husk Charcoal

The rice husk charcoal was treated with hydrochloric acid to remove inorganic impurities and partially open the carbon structure. The charcoal and HCl solution were mixed at a 1:1 mass ratio, followed by stirring at 250 rpm for 1 h at approximately 27 °C. The suspension was then allowed to stand for 24 h to promote acid penetration and impurity leaching. After treatment, the solid fraction was separated by filtration and washed repeatedly with deionized water until the filtrate reached a neutral pH. The washed material was dried at 100 °C for 1 h and subsequently heated at 500 °C for 1 h to obtain activated rice husk carbon. This sequential acid and thermal treatment was intended to reduce ash-forming impurities while improving the accessibility of the carbon surface [10].

2.4. Plasma-Assisted Surface Modification

The plasma modification was performed using an argon plasma jet powered by a high-voltage power supply (Chemical Engineering Laboratory, Universitas Negeri Semarang, Semarang, Indonesia). The system employed a stainless-steel rod electrode, 0.15 cm in diameter, positioned inside a glass tube with outer and inner diameters of 0.5 and 0.4 cm, respectively. An aluminium ribbon connected to the ground terminal functioned as the ground electrode. The distance between the electrodes was fixed at 8 cm, and the ground electrode was positioned 0.3 cm from the plasma jet outlet. The power supply operated within a voltage range of 0–20 kV, while the plasma treatment was conducted under an argon flow rate of 3 L min^{-1}, an operating voltage of 5.5 kV, and a frequency of 20 kHz [11].

2.5. Nitrogen Functionalization Using Ammonia Gas

Nitrogen functionalization was performed by exposing the plasma-modified activated carbon to ammonia under a controlled thermal atmosphere. The reactor (Chemical Engineering Laboratory, Universitas Negeri Semarang, Semarang, Indonesia) was purged with argon to remove residual oxygen and moisture. The sample was then heated to 200 °C and maintained for 20 min under NH_3 flow at 100 sccm, while the chamber pressure was maintained at atmospheric pressure, depending on the reactor configuration. After treatment, the NH_3 supply was stopped, and the reactor was purged with argon until the exhaust gas was safely removed [12].

2.6. Preparation of Nitrogen-Functionalized Rice Husk Carbon/$LiMn_2O_4$ Composite

The nitrogen-functionalized rice husk carbon was incorporated into commercial $LiMn_2O_4$ powder as a conductive and surface-modifying carbon additive. Three composite formulations were prepared by adding the nitrogen-functionalized rice husk-derived carbon loadings at 2, 3, and 4 wt.% relative to the mass of $LiMn_2O_4$. The samples were coded as LMO-NC2, LMO-NC3, and LMO-NC4, respectively. Each mixture was homogenized by ball milling (Chemical Engineering Laboratory, Universitas Negeri Semarang, Semarang, Indonesia) at 300 rpm for 2 h to improve the physical distribution of the carbon phase within the $LiMn_2O_4$ [13]. All experiments were carried out in triplicate under identical processing conditions. For each sample formulation, three independent preparations were conducted, and the resulting data were averaged to improve reliability and reduce random experimental variation.

Tabel 1. Experimental design

Sample code	Nitrogen-functionalized rice husk carbon loadings	Milling speed	Milling time
LMO-NC2	2 wt.%	300 rpm	2 h
LMO-NC3	3 wt.%	300 rpm	2 h
LMO-NC4	4 wt.%	300 rpm	2 h

2.7. Characterization

The prepared LMO-NC composites were characterized to examine their surface chemistry, morphology, crystalline structure, and textural properties. Fourier-transform infrared spectroscopy (FTIR) was performed in the range of 4000–400 cm^{-1} using an FTIR spectrometer (PerkinElmer Frontier, USA) to identify functional groups related to O–H, C=C, C=N, Si–O, and Mn-O vibrations [14]. Surface morphology was observed using scanning electron microscopy (SEM) (Phenom, Thermo Fisher Scientific, USA) at 15 kV and 10,000× magnification. The SEM images were used to evaluate layered $LiMn_2O_4$, fine carbonaceous deposits, interparticle voids, and agglomeration [15]. X-ray diffraction (XRD) (Philips X'pert PRO, Netherlands) with Cu Kα radiation, λ = 1.5406 Å, over a 2θ range of 10–75°. The diffraction peaks were compared with standard spinel $LiMn_2O_4$ patterns [16]. Textural properties were analyzed using BET surface area analysis (Quantachrome Instruments, USA) after degassing at 300 °C [17].

3. Results and Discussion

3.1. FTIR Spectra Analysis

The FTIR spectra of LMO-NC2, LMO-NC3 and LMO-NC4 are shown in Figure 1.

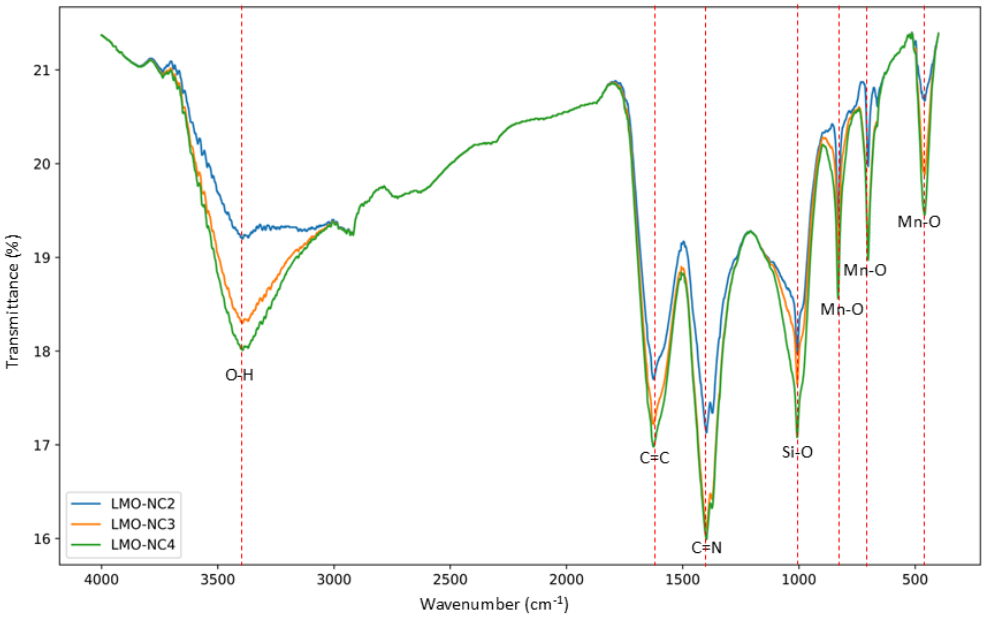

Figure 1. FTIR spectra of $LiMn_2O_4$ composites with different nitrogen-functionalized rice husk-derived carbon loadings.

Figure 1 illustrated the FTIR spectra of LMO-NC2, LMO-NC3, and LMO-NC4 exhibit broadly similar spectral features, indicating that the incorporation of 2, 3 and 4 wt.% nitrogen-functionalized rice husk-derived carbon loadings did not substantially alter the main chemical framework of the $LiMn_2O_4$-based composites. The broad band at 3390 cm^{-1} is assigned to O–H stretching vibrations from surface hydroxyl groups or adsorbed moisture. The band at 1625 cm^{-1} may be attributed to C=C stretching of carbon domains.

The intense band around 1400 cm^{-1} is tentatively associated with C=N-related vibrations, suggesting the contribution of nitrogen-containing surface functionalities from the nitrogen-functionalized rice husk-derived carbon phase. Meanwhile, the band around 1000 cm^{-1} may correspond to Si–O vibrations, which is reasonable considering the rice-husk origin of the carbon additive. The bands in the lower wavenumber region, particularly between 800 and 400 cm^{-1}, are mainly attributed to Mn–O lattice vibrations of the spinel $LiMn_2O_4$. A decrease in minimum transmittance was observed for several bands as the nitrogen-functionalized rice husk carbon loadings increased from LMO-NC2 to LMO-NC4. This trend has been reported by Bunyamin et al. indicates stronger relative absorption associated with surface functional groups and carbon-derived features in the higher-carbon composites [18]. At the same time, the persistence of Mn–O-related bands confirms that the characteristic $LiMn_2O_4$ framework remained detectable after composite preparation [19]. This according to Asuti et al., the FTIR results suggest that nitrogen-functionalized rice husk-derived carbon mainly modified the surface chemical features of the composites while preserving the main $LiMn_2O_4$-related metal–oxygen vibration [20].

3.2. SEM Morphological Analysis of LMO-NC Composites

The SEM micrographs of LMO-NC2, LMO-NC3, and LMO-NC4 are presented in Figure 2.

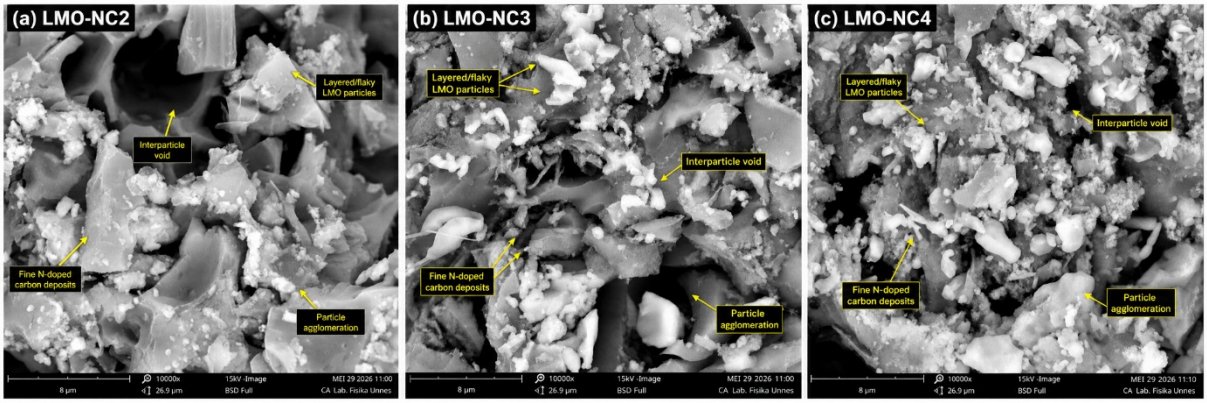

Figure 2. SEM images of LMO-NC composites with different nitrogen-functionalized rice husk-derived carbon loadings : (a) LMO-NC2, (b) LMO-NC3, and (c) LMO-NC4

Based from Figure 2 (a), the morphology of LMO-NC2 is dominated by relatively large layered $LiMn_2O_4$ with limited fine deposits on the surface. This indicates that at 2 wt.% carbon loading, the amount of nitrogen-functionalized rice husk-derived carbon loadings was relatively low and did not fully cover the particle surfaces. The presence of interparticle voids suggests that the particles were not completely compacted, which may be beneficial for electrolyte access in future electrochemical applications. However, the lower amount of carbon may provide fewer interparticle conductive contact points compared with samples containing higher carbon loading [21].

Figure 2 (b) shows a more balanced morphology of LMO-NC3. The fine nitrogen-functionalized rice husk-derived carbon loadings deposits appear more widely distributed among the layered $LiMn_2O_4$, while the structure remains visible. This suggests that 3 wt.% carbon loading may provide better dispersion of the carbon phase without excessive agglomeration. From a composite-design perspective, this morphology is favorable because the carbon additive may improve particle-to-particle contact while maintaining the visible structural characteristics of the $LiMn_2O_4$ [22]. Figure 2 (c) illustrated the surface appears to contain more abundant fine deposits and more pronounced particle agglomeration of LMO-NC4. This is consistent with the higher carbon loading of 4 wt.%, which increases the probability of carbon-rich regions forming between and on the surface of $LiMn_2O_4$. Although higher carbon loading may improve physical contact among particles, excessive agglomeration can reduce dispersion uniformity and may limit effective interfacial contact if carbon clusters are not evenly distributed. Therefore, increasing carbon content does not automatically produce a better morphology; the distribution quality of the carbon phase is critical [23].

The SEM images suggest a gradual morphological evolution from LMO-NC2, LMO-NC3 and LMO-NC4. LMO-NC2 shows lower visible carbon deposition, LMO-NC3 displays relatively balanced carbon distribution, and LMO-NC4 exhibits more intense agglomeration and denser carbon-rich regions. This trend is consistent with Perumat et al., the increasing nitrogen-functionalized rice husk-derived carbon loadings from 2, 3 and 4 wt.%. The observed interparticle voids and heterogeneous particle arrangement may support material accessibility [24].

3.3. XRD Analysis of LMO-NC Composites

The XRD patterns of LMO-NC2, LMO-NC3, and LMO-NC4 are presented in Figure 3.

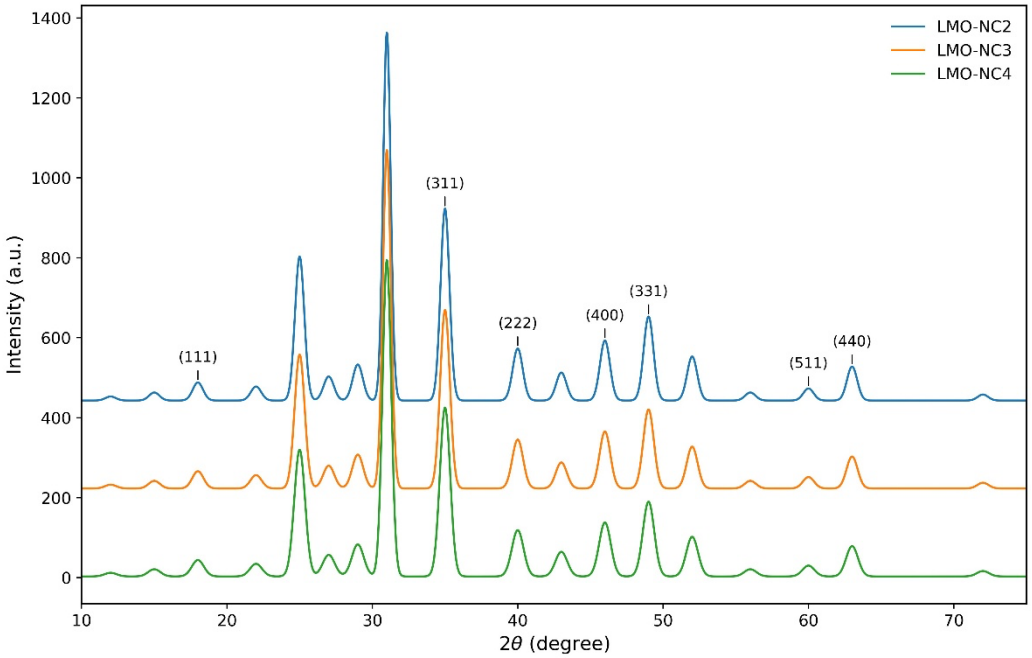

Figure 3. XRD patterns of LMO-NC2, LMO-NC3, and LMO-NC4 composites

Figure 3 illustrated the peak around 35° assigned to the (311) plane and the reflections in the regions of 40°, 46°, 49°, 60°, and 63° corresponding to the (222), (400), (331), (511), and (440) planes, respectively, are consistent with the typical diffraction characteristics of cubic spinel $LiMn_2O_4$. The persistence of these peaks suggests that the incorporation of the nitrogen-functionalized rice husk-derived carbon phase did not destroy the crystalline framework of the active $LiMn_2O_4$.

A strong diffraction feature was also observed around 31°, which showed the highest relative intensity in the LMO-NC2 pattern. However, this peak is not directly assigned in the present discussion

because its position does not correspond clearly to the main characteristic reflection commonly emphasized for spinel $LiMn_2O_4$ in the simplified indexing scheme used here [25]. The overall similarity in peak positions among LMO-NC2, LMO-NC3, and LMO-NC4 indicates that variation in nitrogen-functionalized rice husk-derived carbon loadings mainly affected the relative intensity rather than the fundamental crystal structure. This is reasonable because the carbon additive, especially when introduced in a relatively small proportion, is usually poorly crystalline or partially amorphous and therefore does not produce dominant sharp diffraction peaks [26]. Instead, its presence may reduce the relative intensity of $LiMn_2O_4$ peak sharpness due to changes in the composite matrix and dilution of the crystalline oxide fraction. This results according to Nyamaa et al. suggest that $LiMn_2O_4$ remained the dominant crystalline phase in the composites, while the nitrogen-functionalized rice husk rice husk carbon loadings acted mainly as a secondary component [27].

3.4. BET Surface Area and Adsorption–Desorption Behavior

The nitrogen adsorption–desorption isotherms of LMO-NC2, LMO-NC3, and LMO-NC4 are shown in Figure 4.

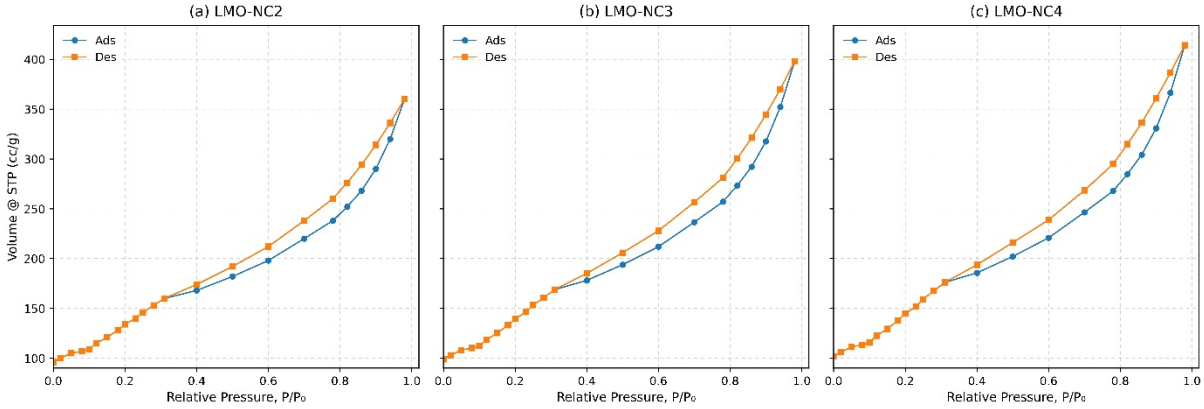

Figure 4. N_2 adsorption–desorption isotherms of LMO-NC2, LMO-NC3, and LMO-NC4 composites

Figure 4 (a) illustrated the adsorption volume increased steadily as P/P_0 increased, indicating that the LMO-NC2 possessed accessible surface sites and pore channels. Its adsorption capacity was lower than those of LMO-NC3 and LMO-NC4. This suggests that the lower nitrogen-functionalized rice husk carbon loading in LMO-NC2 provided a smaller contribution to pore accessibility and total adsorbed volume. Figure 4 (b) showed a higher adsorption–desorption volume of LMO-NC3 than LMO-NC2 across the relative pressure range. This indicates that increasing the nitrogen-functionalized rice husk-derived carbon loading content to 3 wt.% improved the textural contribution of the composite. The moderate separation between adsorption and desorption branches suggests improved pore accessibility while maintaining a relatively balanced morphology. This result is consistent with Bunyamin et al., where LMO-NC3 showed a more even distribution of fine carbon deposits among the $LiMn_2O_4$ [18]. Figure 4 (c) exhibited the highest adsorption and desorption volumes of LMO-NC4 among the three samples. The higher uptake can be attributed to the increased amount of nitrogen-functionalized rice husk-derived carbon loading, which may contribute additional accessible surface sites and pore volume. The result according to Astuti et al. reported the larger separation between adsorption and desorption branches also suggests stronger pore-related hysteresis, which may be associated with mesoporous structures, interparticle voids, or agglomerated carbon-rich regions [20].

4. Conclusion

This study demonstrated the preparation and characterization of $LiMn_2O_4$ composites containing nitrogen-functionalized rice husk-derived carbon at different loadings. The incorporation of 2, 3, and 4 wt.% nitrogen-functionalized rice husk-derived carbon loadings produced LMO-NC2, LMO-NC3, and LMO-NC4 composites with distinguishable surface, morphological, crystalline, and textural characteristics. These results suggest that the N-functionalized rice husk carbon contributed to the surface chemistry of the composites while the $LiMn_2O_4$ remained detectable. The characteristic reflections assigned to the $LiMn_2O_4$ indicate that carbon incorporation did not substantially disrupt the crystalline framework of the cathode material. The findings confirm that nitrogen-functionalized rice husk carbon can serve as a sustainable secondary phase for modifying the physicochemical and textural properties of $LiMn_2O_4$. However, the present work remains at the material-characterization stage. Electrochemical testing, including charge–discharge cycling, rate capability, cyclic voltammetry, and impedance analysis, is required to verify whether these structural and surface modifications translate into improved cathode performance.

Declaration of AI and AI assisted technologies in the writing process

The author(s) declare that no artificial intelligence (AI) or AI-assisted technologies were used in the preparation, writing, or editing of this manuscript. All aspects of the work were conducted and written solely by the author(s).

Declaration of Competing Interest

The authors declare that they have no known competing interests that could have appeared to influence the work reported in this paper.

Acknowledgment

The authors gratefully acknowledge the Faculty of Engineering, Universitas Negeri Semarang, for the providing financial support for this research under contract number 111.4.5/UN37/PPK.05/2026.

References

[1] Y. Chen, Z. Xia, L. Huang, L. Cui, X. Gao, M. Niu, X. Chen, D. Zhou, Z. Guo, T. Hu, X. Chen, O. Breuer, M. Fayena-Greenstein, D.-J. Lee, D. Aurbach, and G. Wang, "Engineering Multifunctional Conductive Carbon-Based Cathode Additives to Stabilize High-Performance All-Solid-State Lithium Metal Batteries," Mater. Today, vol. 88, pp. 368–381, 2025, doi: https://doi.org/10.1016/j.mattod.2025.07.007.

[2] T. Khandaker, T. Islam, A. Nandi, M. A. A. M. Anik, M. S. Hossain, M. K. Hasan, and M. S. Hossain, "Biomass-Derived Carbon Materials for Sustainable Energy Applications: A Comprehensive Review," Sustain. Energy Fuels, vol. 9, no. 3, pp. 693–723, 2025, doi: https://doi.org/10.1039/D4SE01393J.

[3] Z. Chen, X. Wang, B. Xue, W. Li, Z. Ding, X. Yang, J. Qiu, and Z. Wang, "Rice Husk-Based Hierarchical Porous Carbon for High Performance Supercapacitors: The Structure-Performance Relationship," Carbon, vol. 161, pp. 432–444, 2020, doi: https://doi.org/10.1016/j.carbon.2020.01.088.

[4] S. Anis, J. Bale, S. E. Cahyanto, N. Kurniadi, D. F. Fitriyana, M. T. Anwar, J. P. Siregar, and N. F. D. S. Guterres, "Effect of Biomass Feedstock Granulometry on Thermophysical Characteristics of Charcoal Briquettes via Screw Extrusion," Adv. Sustain. Sci. Eng. Technol., vol. 7, no. 4, p. 02504034, 2025, doi: https://doi.org/10.26877/asset.v7i4.2047.

[5] P. Venkatachalam, N. Murugan, K. Dhanabalan, M. Kang, Y. Kim, H.-Y. Jung, and Y. A. Kim, "Hierarchical Porous Carbon Nanosheets Derived from Rice Husk as Coating Layer for the

Anode of Lead-Carbon Battery," J. Power Sources, vol. 657, p. 238168, 2025, doi: https://doi.org/10.1016/j.jpowsour.2025.238168.
[6] D. F. Fitriyana, A. E. Hadi, N. Suhodo, A. Bahatmaka, J. P. Siregar, T. Cionita, Z. A. S. Bahlawan, and A. Y. Maulana, "Effect of Printing Speed on the Properties of 3D Printed Products Using Recycled PET Filament," Adv. Sustain. Sci. Eng. Technol., vol. 8, no. 3, p. 0260302, 2026, doi: https://doi.org/10.26877/asset.v8i3.2049.
[7] Y. Niu, C. Zheng, Y. Xie, K. Kang, H. Song, S. Bai, H. Han, and S. Li, "Efficient Adsorption of Ammonia by Surface-Modified Activated Carbon Fiber Mesh," Nanomaterials, vol. 13, no. 21, p. 2857, 2023, doi: https://doi.org/10.3390/nano13212857.
[8] N. Qudus, H. Harianingsih, D. F. Fitriyana, V. A. Kristianto, D. Gustoro, N. Khoirunisa', K. Saputra, J. Jaafar, J. P. Siregar, and S. Palanisamy, "Effect of Calcination Temperature and Impregnation Time on Physicochemical and Textural Properties of KOH-Modified Rice Husk Ash Materials," J. Compos. Sci., vol. 10, no. 6, p. 290, 2026, doi: https://doi.org/10.3390/jcs10060290.
[9] A. H. Wazir, I. U. Wazir, and A. M. Wazir, "Preparation and Characterization of Rice Husk Based Physical Activated Carbon," Energy Sources Part A Recover. Util. Environ. Eff., pp. 1–11, 2020, doi: https://doi.org/10.1080/15567036.2020.1715512.
[10] N. Hossain, S. Nizamuddin, P. Selvakannan, G. Griffin, S. Madapusi, and K. Shah, "The Effect of KOH Activation and Ag Nanoparticle Incorporation on Rice Husk-Based Porous Materials for Wastewater Treatment," Chemosphere, vol. 291, p. 132760, 2022, doi: https://doi.org/10.1016/j.chemosphere.2021.132760.
[11] H. Harianingsih, A. N. D. Indriawan, R. Setiadi, I. S. Pangestu, I. N. Ubay, and S. R. Erliana, "The Improvement of Modified Rice Straw Fiber/Polyvinyl Alcohol Thermoplastic Polymer Composite Using Cold Plasma Technology," Indones. J. Chem., vol. 24, no. 4, pp. 1145–1155, 2024, doi: https://doi.org/10.22146/ijc.93255.
[12] H. Harianingsih, W. Astuti, C. R. Widyastuti, R. Wulandari, and A. A. Puzi, "Surface Treatment of Wood Polymer Composites from Straw Fiber Using Argon Plasma Jet Injection: Enhancing Adhesion Properties," J. Bahan Alam Terbarukan, vol. 13, no. 2, pp. 108–116, 2025, doi: https://doi.org/10.15294/jbat.v13i2.5572.
[13] A. K. M. Selim, I. Ayyubov, E. Tálas, I. Borbáth, and A. Tompos, "Functionalized Carbon Nanostructures for PEMFCs: Catalyst and Membrane," in Handbook of Functionalized Carbon Nanostructures, A. Barhoum and K. Deshmukh, Eds. Cham, Switzerland, 2024, pp. 1–51, doi: https://doi.org/10.1007/978-3-031-14955-9_76-1.
[14] T. Kopac, "Hydrogen Storage Characteristics of Bio-Based Porous Carbons of Different Origin: A Comparative Review," Int. J. Energy Res., vol. 45, no. 15, pp. 20497–20523, 2021, doi: https://doi.org/10.1002/er.7130.
[15] V. V. Korobochkin, N. V. Tu, and N. M. Hieu, "Production of Activated Carbon from Rice Husk Vietnam," IOP Conf. Ser. Earth Environ. Sci., vol. 43, p. 012066, 2016, https://doi.org/10.1088/1755-1315/43/1/012066.
[16] A. U. Elinwa, "X-Ray and Microstructure of Rice Husk Ash-Admixed Concrete," preprint, In Review, Nov. 2023, doi: https://doi.org/10.21203/rs.3.rs-3630083/v1.
[17] L. Rumiyanti, S. Gracia, N. I. Istiqomah, D. A. Larasati, Y. D. Prabowo, N. P. Rini, W. Andriyanti, P. Manurung, A. Sharma, D. Ali, Chotimah, and E. Suharyadi, "A Sustainable and Eco-Friendly Rice Husk-Derived Mesoporous Silica Nanoparticles Loaded with Benzotriazole for Enhanced Corrosion Inhibition," Biomass Bioenergy, vol. 203, p. 108335, 2025, doi: https://doi.org/10.1016/j.biombioe.2025.108335.
[18] Bunyamin, I. Winaningsih, D. F. Fitriyana, S. W. Wibowo, R. I. Fadzillah, and H. Harianingsih, "Physicochemical Characterization of KOH-Activated Rice Husk-Derived Carbon toward Sustainable Anode Materials for Lithium-Ion Batteries," Appl. Chem. Eng., 2026, doi: https://doi.org/10.59429/ace.v9i1.5891.

[19] U. Latif, “Comprehensive Review of Li-Oxygen Batteries: Electrolytes, Electrodes, Redox Mediators, and Thermodynamics,” ACS Appl. Energy Mater., vol. 8, no. 8, pp. 4838–4883, 2025, doi: https://doi.org/10.1021/acsaem.4c03144.

[20] P. Astuti, A. J. W. Nouvaldi, A. Rahmayanti, P. S. Shabura, M. E. F. Adzani, D. A. Tsany, A. Y. Purnama, and R. S. Rafdinal, “Geopolymer Bio-Patch Repair: Microbially-Induced Calcite and Pozzolanic Fly Ash and Rice Husk Ash for Corrosion-Resistant of Reinforced Concrete Repair,” Adv. Sustain. Sci. Eng. Technol., vol. 8, no. 1, p. 02601040, 2026, doi: https://doi.org/10.26877/asset.v8i1.2729.

[21] X. Lu, G. J. Lian, J. Parker, R. Ge, M. K. Sadan, R. M. Smith, and D. Cumming, “Effect of Carbon Blacks on Electrical Conduction and Conductive Binder Domain of Next-Generation Lithium-Ion Batteries,” J. Power Sources, vol. 592, p. 233916, 2024, doi: https://doi.org/10.1016/j.jpowsour.2023.233916.

[22] Y. Abe, M. Tomioka, M. Kabir, and S. Kumagai, “Role of SiOx in Rice-Husk-Derived Anodes for Li-Ion Batteries,” Sci. Rep., vol. 12, no. 1, p. 975, 2022, doi: https://doi.org/10.1038/s41598-022-04979-5.

[23] S. Wang, W. Hu, M. Zhou, Y. Gao, Q. Deng, Y. Mao, Q. Xu, and G. Wang, “Synergistic Effects of Microstructures and Active Nitrogen Content on the Oxygen Reduction Reaction Performance of Nitrogen-Doped Carbon Nanofibers via KOH Activation Heat Treatment,” J. Mater. Sci., vol. 55, no. 24, pp. 10725–10739, 2020, doi: https://doi.org/10.1007/s10853-020-04673-9.

[24] J. Liu, K. Zhang, H. Wang, L. Lin, J. Zhang, P. Li, Q. Zhang, J. Shi, and H. Cui, “Advances in Micro-/Mesopore Regulation Methods for Plant-Derived Carbon Materials,” Polymers, vol. 14, no. 20, p. 4261, 2022, doi: https://doi.org/10.3390/polym14204261.

[25] N. N. Ngoc, L. X. Thanh, L. T. Vinh, and B. T. V. Anh, “High-Purity Amorphous Silica from Rice Husk: Preparation and Characterization,” Vietnam J. Chem., vol. 56, no. 6, pp. 730–736, 2018, doi: https://doi.org/10.1002/vjch.201800079.

[26] H. H. Hval and H. Fjellvåg, “Tracking Phase Transformations in LiMn1.5+xNi0.5−xO4 by High Resolution X-Ray Diffraction,” J. Mater. Chem. A, vol. 13, no. 47, pp. 41122–41143, 2025, doi: https://doi.org/10.1039/D5TA05130D.

[27] O. Nyamaa, G.-H. Kang, S.-C. Huh, J.-H. Yang, T.-H. Nam, and J.-P. Noh, “Unraveling the Mechanism and Practical Implications of the Sol-Gel Synthesis of Spinel $LiMn_2O_4$ as a Cathode Material for Li-Ion Batteries: Critical Effects of Cation Distribution at the Matrix Level,” Molecules, vol. 28, no. 8, p. 3489, 2023, doi: https://doi.org/10.3390/molecules28083489.